Effect of filler types on the performance of porous asphalt pavement using a coupled multiscale finite element method

Cong Du, Ph.D. Student, Graduate Research Assistant [1]; Guoyang Lu, Ph.D., Research Assistant [2]; Haopeng Wang, Ph.D. Student, Graduate Research Assistant [3]; Yiren Sun, Ph.D., Research Assistant [4]; Pengfei Liu, Ph.D., Research Assistant [5]; Dawei Wang, Professor [6]; Sabine Leischner, Ph.D., Research Assistant [7]; Markus Oeser, Professor [8]

[1] Institute of Highway Engineering, RWTH Aachen University, Aachen, 52074, Germany.
Email: du@isca.rwth-aachen.de

[2] Corresponding Author, Institute of Highway Engineering, RWTH Aachen University, Aachen, 52074, Germany.
Email: lu@isca.rwth-aachen.de

[3] Faculty of Civil Engineering and Geosciences, Delft University of Technology, Delft, The Netherlands.
E-mail: haopeng.wang@tudelft.nl

[4] School of Transportation and Logistics, Dalian University of Technology, Dalian 116024, China.
Email: sunyiren@dlut.edu.cn

[5] Corresponding Author, Institute of Highway Engineering, RWTH Aachen University, Aachen, 52074, Germany.
Email: liu@isca.rwth-aachen.de

[6] School of Transportation Science and Engineering, Harbin Institute of Technology, 150090, Harbin, China; Institute of Highway Engineering, RWTH Aachen University, Aachen, 52074, Germany.
Email: wang@isca.rwth-aachen.de

[7] Institute of Urban and Pavement Engineering, Technische Universität Dresden, 01187, Dresden, Germany.
Email: sabine.leischner@tu-dresden.de

[8] Institute of Highway Engineering, RWTH Aachen University, Aachen, 52074, Germany.
Email: oeser@isca.rwth-aachen.de

Abstract

The porous asphalt (PA) pavements are widely employed in the areas with wet climate due to their excellent permeability and superior performance. As particle enhancement inclusions in asphalt mastic, the mineral fillers play essential roles in improving the performance of PA pavements. This study developed a coupled multiscale finite element (FE) model including the mesoscale of PA mixture and the macroscale of PA pavement. Within this model, the mesoscale structure was captured by the X-ray computer tomography (X-ray CT) scanning and reconstructed by the digital image processing (DIP) technology. Four types of mastic properties respectively with four mineral fillers (Granodiorite, Limestone, Dolomite and Rhyolite) were employed in the mesoscale part of pavement model to analyze the effects of filler types on the performance of pavements. A constant tire loading was applied and two temperatures (0 °C and 50 °C) were specified. The performances (load-bearing capacity, rutting resistance and raveling resistance) of pavements with different fillers were identified and ranked, and their correlations with the types and chemical components of fillers were analyzed. The computational results showed that pavements with Rhyolite and Granodiorite fillers have higher load-bearing capacities and rutting resistance, while the Limestone and Dolomite fillers can improve the raveling resistance of the PA pavements. In addition, the chemical components of Al_2O_3 and SiO_2 play dominate roles in improving the load-bearing capacities and rutting resistance of the PA pavements, and the fillers with high percentages of CaO can improve the raveling resistance of the PA pavements. Based on this algorithm, it is possible to select optimal filler for a specific pavement design and thus improve the durability of the PA pavements.

Keywords: porous asphalt pavement; multiscale finite element model; mineral filler; correlation analysis; chemical components

1. Introduction

Due to the superior ability in improving the driving safety during wet weather, porous asphalt (PA) is broadly used as an innovative surfacing technology throughout the world. The open structure of PA offers excellent capabilities for permeating water from the surface as well as reducing noise from highway traffic, and hence improving riding quality and visibility especially in wet conditions (Alber et al. 2018, Lu et al. 2019a, Lu et al. 2019b). However, the high percentage of air void content significantly affects the strength of the PA layers, and hence, the stresses generated by traffic loads have a profound effect on the durability of PA pavements. Moreover, the open structures make it difficult to deeply investigate the mechanical performance of PA pavements. The mechanical performance of PA mixture is not only related to the fundamental material properties, but also its geometric feature at mesoscale (Mohd et al. 2018, Qian et al. 2020). Improving the understanding of the mechanism of PA can significantly promote the structural design approaches, and a long-life higher performance pavement infrastructure can therefore be established.

The mineral filler is wildly employed as a common practice to enhance performance-related properties of asphaltic materials. Researches have proved that the filler plays a dual role in asphalt mixture, which respectively are particle enhancement inclusion and active interfacial material (Kim et al. 2004, Cardone et al. 2015). In particular, for PA in which the strength is mainly provided by coarse aggregate interaction, fillers play an essential role in increasing the viscosity of asphalt mastic for binding the coarse aggregates and preventing the movement of aggregates particles. To date, numerous experimental studies have been conducted to investigate the effects of the mineral fillers on the mechanical and damage properties of the asphalt mastic and mixtures. Rochlani et al. (2019) investigated and compared the rheology properties as well as the fatigue, rutting and low-temperature cracking susceptibility of bitumen with four different filler types (dolomite, granodiorite, limestone and rhyolite). Rieksts et al. (2018) conducted the dynamic shear rheometer (DSR) test on the mastic with three different mineral fillers; the experimental results provide the mastic performance in terms of permanent deformations. In terms of the surface free energy, Alvarez et al. (2019) assessed the effect of fillers on the response of asphalt-aggregate interfaces, and the result led to recommend an optimum range of filler volumetric concentrations. In addition, the effects of fillers on the fracture and fatigue properties of asphalt mastic and asphalt mixture were also investigated by scholars (Al-Hdabi et al. 2014, Fonseca et al. 2019, Stewart et al. 2019, Roberto et al. 2020). As mentioned above, the mineral fillers can enhance the performance of asphalt mastic and mixture, and the effects of the fillers are significantly influenced by their types, volume concentration as well as gradations.

However, the numerical study focusing on the mechanical performance of the PA mixtures and PA pavements influenced by different fillers is seldom reported in the literature. In the past numerical studies on the mechanical response of asphalt mixtures, according to the morphological theory, the multi-phase asphalt mixture, including bitumen, fillers and aggregates, were regarded as a homogeneous material due to the limitation of computation capacity. In fact, the influence of the heterogeneous feature of asphalt mixtures is non-negligible especially for the PA mixtures in which the air void content is larger than 10% (Alvarez et al. 2011, Liu et al. 2011, Liu et al. 2012). Thus, investigations on the mesoscale structure of PA mixtures can provide a deep insight into the stress-strain relations in pavement.

Currently, two approaches are employed to establish the mesoscale models of multiphase composites: random generation algorithm and digital image processing (DIP) technology. The random generation is regarded as the efficient method without extensive labor work. Based on the random take-and-place method, polygon inclusions with various shapes, locations and orientations can be specified and distributed around the matrix (Liu et al. 2018b). Therefore, it is much convenient for scholars to establish the multi-phase models for numerical simulation. Researches have employed this approach to investigate the mechanical behavior of asphalt mixture at mesoscale. For examples, Wang et al. (2014) analyzed the fracture performance of asphalt mixture using the randomly generated 2-dimensional microstructure models, in which the cohesive zone model (CZM) theory and extensive finite element method (XFEM) were utilized to represent the crack initiations. In conjunction with the CZM, Yin et al. (2012) investigated the tensile strength of asphalt mixture based on the heterogeneous model developed with the combination of the aggregate generation and packing algorithm.

However, the inner structure of asphalt mixture is closely relied on the laboratory mixing and compacting process, and thus the random generation models are untenable to represent the aggregates distribution and orientations at mesoscale. To address this issue, the DIP method is based on the digital image of specimens, and can establish the mesoscale structure of the real asphalt mixture. Afterwards, finite element methods (FEM) (Dai et al. 2005, Liu et al. 2018a, Kollmann et al. 2019, Sun et al. 2019, Sun et al. 2020) and discrete element methods (DEM) (Li et al. 2019, Zhang et al. 2019) can be incorporated to calculate the mesoscale mechanics of asphalt mixture.

Nonetheless, an asphalt pavement containing tons of inclusions, voids and micro cracks would require a large amount of mesh element. Therefore, it is unrealistic to conduct a time-consuming and device-related mesoscale simulation on the entire asphalt pavement. As a remedy, an innovative approach that both the mesoscale structure of asphalt mixture and the macroscale structure of asphalt pavement can be simultaneously modeled in the finite element (FE) simulation (Wollny et al. 2020). Within this configuration, the mechanical response of asphalt pavement can be precisely demonstrated while considering the details of the inner structure of asphalt mixture.

To investigate the influence of the different mineral fillers on the mechanical performance of the PA pavement, a coupled multiscale FE model was established in FE software ABAQUS in this study. The mesoscale structure model of PA mixture was created based on the CT scanning image, and the mesoscale model was coupled into a macroscale structure of asphalt pavement. Within the mesoscale model, four types of asphalt mastic were employed that respectively contained different types of mineral fillers: Granodiorite, Limestone, Dolomite and Rhyolite. A constant tire loading was applied on the mesoscale region, and the mechanical responses were investigated to demonstrate the effects of the filler types on the performance of the PA pavement.

2. Methodology

2.1. Preparation of the porous asphalt samples

The PA used in this study was a common type with maximum grain size of 8 mm following the German standard ZTV Asphalt-StB 07 (2007). The specimen was mixed of crushed diabase aggregates, mineral filler and bitumen with a 50/70 penetration grade. The detailed mix design is listed in **Table 1**. The PA samples were prepared by Marshall compactor with 50 impacts per side (Rochlani et al. 2019).

Table 1. Mix design of porous asphalt

Component	Grain size (mm)	Mass percentage (%)	Air void content (Vol.-%)
Mineral filler	0-0.063	5.0	-
	0.063-2	15.0	-
Diabase	2-5.6	37.0	-
	5.6-8	43.0	-
Mixture	-	-	26.2

Previous study (Rochlani et al. 2019) has investigated the chemical compositions of the four types of mineral filler, which are listed in **Table 2**.

Table 2. Chemical composition of mineral filler

	Na_2O	MgO	Al_2O_3	SiO_2	K_2O	CaO	TiO_2	Fe_2O_3	others
Granodiorite	3.22	2.44	18.09	61.70	3.42	2.73	1.04	6.35	0.58
Limestone	0.18	2.02	1.29	1.94	0.19	92.97	0.12	0.82	0.46
Dolomite	0.27	26.02	2.26	5.23	0.61	61.97	0.07	1.91	1.60
Rhyolite	1.42	0.41	19.65	65.69	8.98	0.26	0.26	3.04	0.24

Notice that the microstructures of the PA with different types of mineral filler are identical. Therefore, the Granodiorite filler was selected to prepare the PA mixture specimen in order to identify its microstructure. Subsequently, the mastic respectively with the four types of mineral filler were prepared with a binder-filler mass ratio of 1:1.6, and their rheological properties were determined by the strain and frequency sweep tests (Rochlani et al. 2019).

2.2. Development of the coupled multiscale model

As aforementioned, the mesoscale structure of the PA was established based on the digital CT image of the specimen. In terms of the DIP technology, the CT image was firstly converted into the binary one according to its intensity values. Thus the areas of asphalt mortar and aggregates can be separately identified. Subsequently, the coordinates of the vertex of polygonal aggregates and air voids can be determined by incorporating the boundary detection and polygon approximation technologies (Reyes-Ortiz et al. 2019, Xing et al. 2019). Consequently, the mesoscale model of the PA mixture was established in the axisymmetric coordinates based on the parametric modeling method of ABAQUS, which can afford comparable simulation accuracy to the three-dimensional model as well as significantly save the computational time. The mesoscale model was discretized by CAX3 (3-node linear axisymmetric element) and CAX4 (4-node bilinear axisymmetric element), as shown in **Figure 1**.

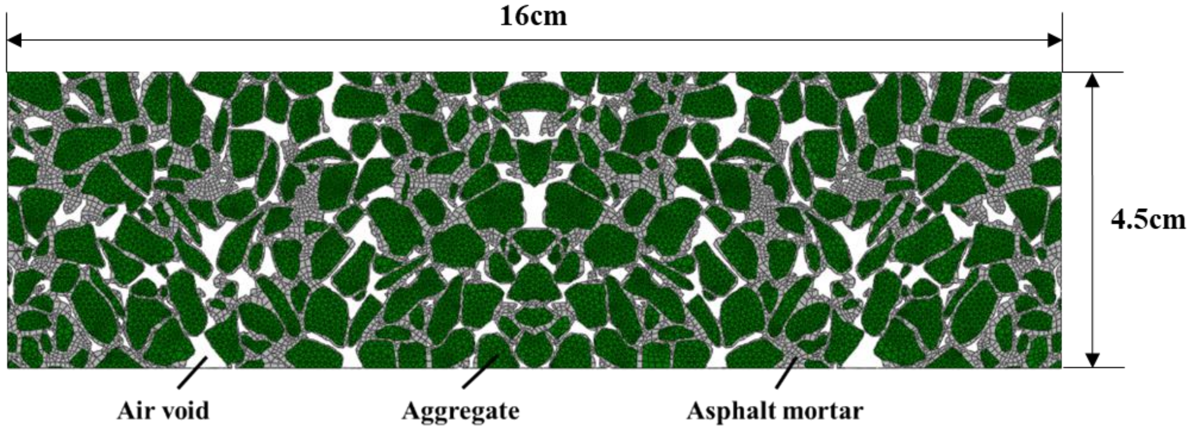

Figure 1 Image of the mesoscale model of porous asphalt mixture

According to the German pavement design specification (1999), the macroscale FE model of PA pavement was developed in the axisymmetric coordinate system, and the loading area was defined as a circle region with a radius of 10cm at center. The macroscale model was discretized by CAX4 elements. The symmetry axis and bottom of the model were respectively restricted in the horizontal and vertical directions. Due to the limitation of the size of the CT image, the mesoscale part of asphalt pavement was selected at the center of the surface layer with a size of 16 cm × 4.5 cm. The coupled multiscale model is presented in **Figure 2**.

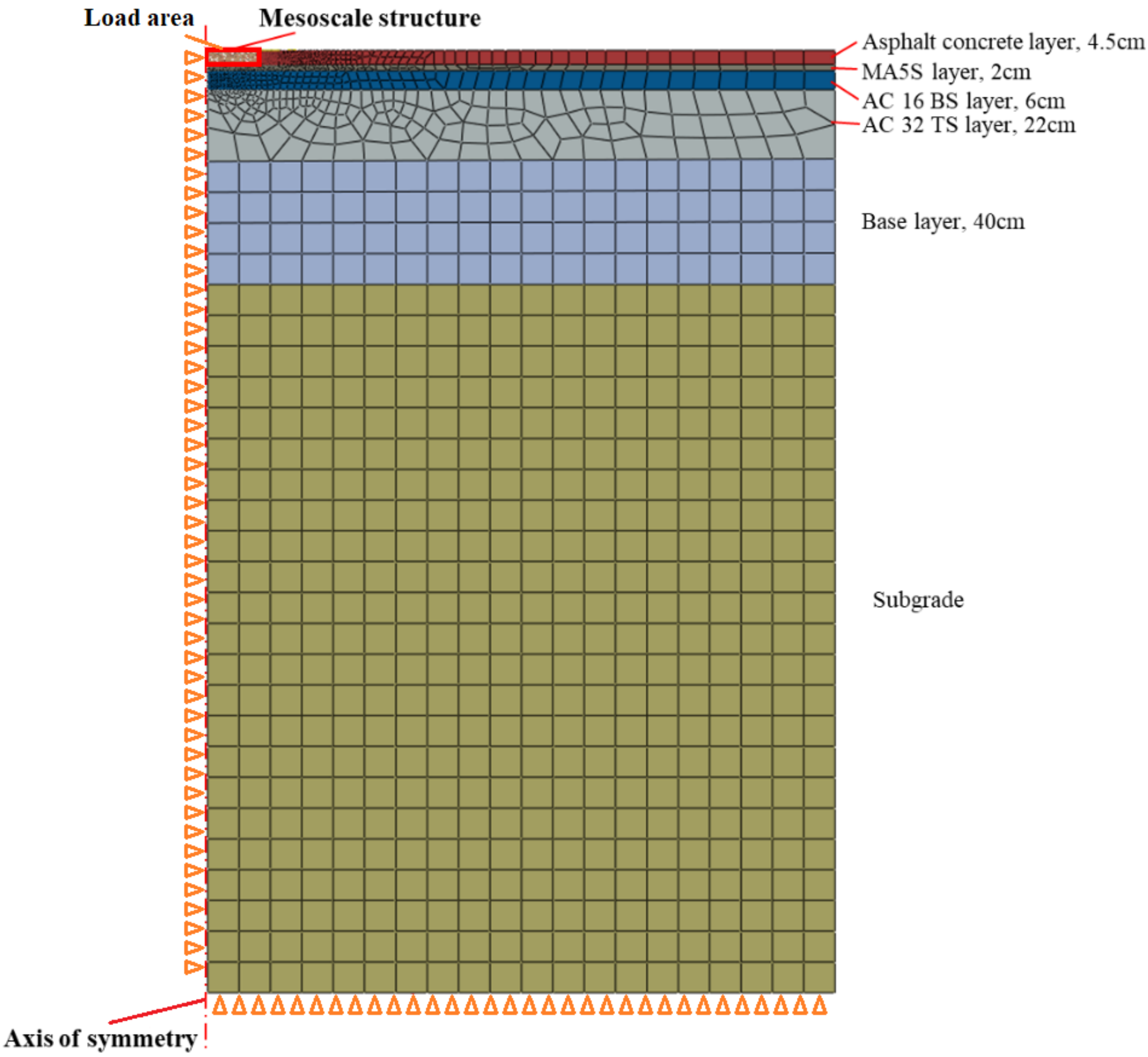

Figure 2 Image of the multiscale model of asphalt pavement

Table 3 lists the model parameters for the mesoscale part, i.e., asphalt mastic and aggregate. The Prony series at 0 °C and 50 °C, which is the classic linear viscoelastic parameters in FE simulation, was specified in the asphalt mastic to represent the time-dependent performance according to previous study (Rochlani et al. 2019). The Young’s modulus and Poisson’s ratio of aggregate were assign in terms of (Kim et al. 2012).**Table 4** lists the parameters for the macroscale part. The linear elastic Young’s modulus of base layer and subgrade were defined in terms of typical values (Sun et al. 2019). In addition, the elastic modulus of MA5S layer, AC 16 BS layer and AC 32 TS layer were assigned as temperature-dependent (1999). For the time-dependent elastic properties of PA layers with different mineral fillers, the Young's modulus and Poisson's ratio were identified based on the calculation of the macro-mechanical responses of the mesoscale model (Allen 2001).

Table 3 Model parameters for mesoscale model

Series	Mastic_Granodiorite				Mastic_Limestone			
	0 °C		50 °C		0 °C		50 °C	
i	ρ_i	E_i(MPa)	ρ_i	E_i(M Pa)	ρ_i	E_i(MPa)	ρ_i	E_i(MPa)
1	7.08E+09	2.34E-03	6.47E+08	9.24E-03	5.25E+05	1.03E+01	8.84E+02	6.89E-03
2	9.05E+05	2.73E+01	1.23E+09	2.39E-03	1.00E+00	1.48E+02	1.05E+03	1.67E-03
3	7.08E+09	2.96E-01	4.57E+08	5.23E-04	8.25E+07	1.01E-02	9.30E+02	6.87E-04
4	1.00E+00	2.30E+02	6.64E+08	1.29E-04	7.00E+09	7.33E-02	9.26E+02	4.93E-04
5	3.16E-07	7.07E+03	3.16E-07	2.00E+03	3.16E-07	7.00E+03	3.16E-07	1.42E+02
6	3.16E-06	3.02E+03	3.16E-06	3.10E+01	3.16E-06	3.85E+03	3.16E-06	1.37E+02
7	3.16E-05	1.19E+03	3.16E-05	4.34E+01	3.16E-05	1.34E+03	3.16E-05	3.19E+01
8	3.16E-04	6.65E+02	3.16E-04	1.44E+01	3.16E-04	6.24E+02	3.16E-04	1.04E+01
9	3.16E-03	5.44E+02	3.16E-03	3.32E+00	3.16E-03	4.62E+02	3.16E-03	2.03E+00
Series	Mastic_Dolomite				Mastic_Rhyolite			
	0 °C		50°C		0 °C		50 °C	
i	ρ_i	E_i(MPa)	ρ_i	E_i(MPa)	ρ_i	E_i(MPa)	ρ_i	E_i(MPa)
1	5.55E+09	2.15E+00	5.13E+03	1.12E-02	5.02E+09	8.38E-03	1.32E+09	1.75E-02
2	1.18E+09	2.14E+00	5.22E+03	3.37E-04	4.99E+09	1.18E-02	1.56E+09	4.55E-03
3	5.10E+09	2.14E+00	5.63E+03	1.50E-03	5.01E+09	1.56E-02	9.36E+08	8.33E-04
4	2.91E+00	1.60E+02	5.11E+03	5.58E-03	2.05E+06	7.80E+01	8.85E+08	1.36E-04
5	3.16E-07	9.62E+03	3.16E-07	1.93E+02	3.16E-07	8.11E+02	3.16E-07	2.28E+03
6	3.16E-06	3.63E+03	3.16E-06	1.93E+02	3.16E-06	1.10E+03	3.16E-06	5.07E+01
7	3.16E-05	1.55E+03	3.16E-05	4.76E+01	3.16E-05	8.95E+02	3.16E-05	5.09E+01
8	3.16E-04	7.26E+02	3.16E-04	1.45E+01	3.16E-04	4.32E+02	3.16E-04	1.82E+01
9	3.16E-03	6.79E+02	3.16E-03	3.19E+00	3.16E-03	5.94E+02	3.16E-03	3.64E+00

All mastics		Aggregate	
E_∞ (MPa)	μ	E(MPa)	μ
3.16E-08	0.30	5.50E+04	0.25

Table 4. Model Parameters for macroscale model

	0°C		50°C	
	E(MPa)	μ	E(MPa)	μ
Asphalt concrete				
Granodiorite	3.67E+04	0.3	5.76E+02	0.3
Limestone	2.51E+04		2.69E+02	
Dolomite	2.81E+04		4.15E+02	
Rhyolite	1.44E+04		6.63E+02	
MA5S layer	2.05E+04	0.35	1.05E+03	0.35
AC 16 BS	2.20E+04	0.35	1.11E+03	0.35
AC 32 TS	1.47E+04	0.35	1.23E+03	0.35
	E(MPa)		μ	
Base layer	1.20E+02		0.49	
Subgrade	4.50E+01		0.49	

In this study, two temperatures (0 °C and 50 °C) were specified on the simulation, and the performance of pavements, including load-bearing capacity, rutting resistance and fatigue cracking resistance, were analyzed. Due to the lower stiffness of PA mixtures at high temperature, the amplitudes of the load were specified as different values for 0 °C and 50 °C simulations, which were 0.7 MPa and 0.0007 MPa, respectively. In addition, the tire loading was assigned to be constant (time=100 s) on the model to simulate the cumulative vehicle load.

3. Results and discussion

3.1. Load-bearing capacity of PA pavement

The deformations at pavement surface in the center of the loading area are shown in **Figure 3**, which reflects the load-bearing capacities of pavement at low and high temperatures.

At 0 °C, the pavement with Rhyolite filler immediately reached and stabilized at the largest value of deformation at very early stage, and was subsequently exceeded by the pavements with the other three fillers, respectively. At the end of the loading time, the pavement with Dolomite filler has the highest deformation value that is 0.293 mm. The second highest value appears in the Limestone enhanced pavement, accounting for deformation of 0.272 mm. The deformations of the Granodiorite and Rhyolite fillers enhanced pavements are 0.193 mm and 0.157 mm, respectively. Hence, it indicates that the capacity of Rhyolite filler enhanced pavement is the highest at the end of the loading period, followed by pavements with Granodiorite and Limestone fillers, and the pavement with Dolomite filler has the lowest capacities. In addition, the deformation of pavements exhibited strong time-dependent properties. In particular, the Dolomite filler enhanced pavement showed the smallest value of deformation at early stage, and it gradually increased and eventually became the largest value at the end of loading, which is remarkably different from the pavement with Rhyolite filler. The distinction might be related to the viscoelastic properties of the PA mixture with different fillers. The PA mixture with Dolomite filler shows more viscos behavior at low temperature, and hence the responses were changing in the entire loading period; however, the PA mixture with Rhyolite filler exhibits more elasticity and responds to the loadings in an extremely short period. This different is believed to closely relate to the chemical components of the mineral filler, which will discuss later.

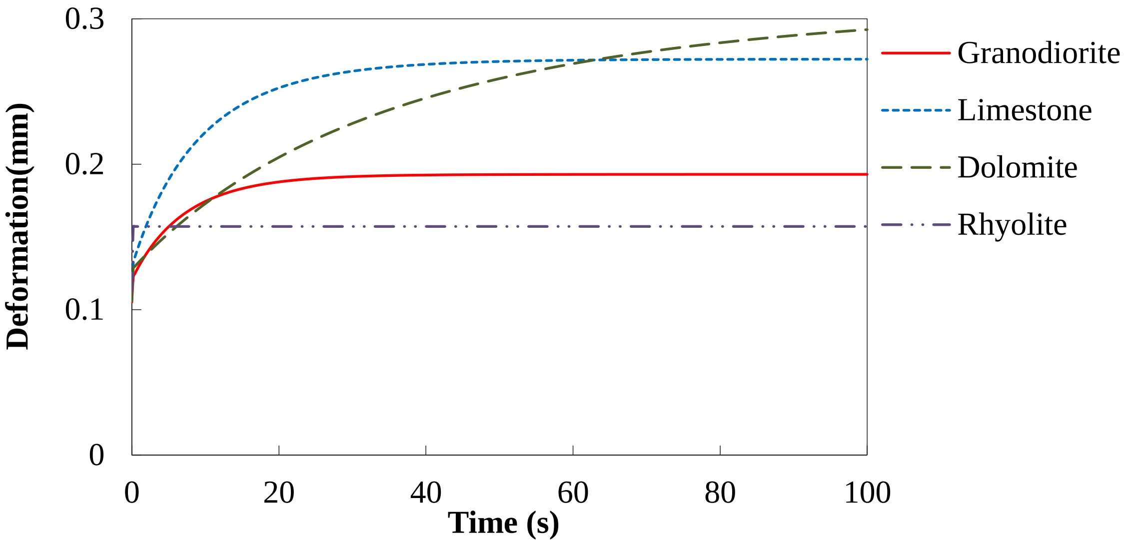

(a)

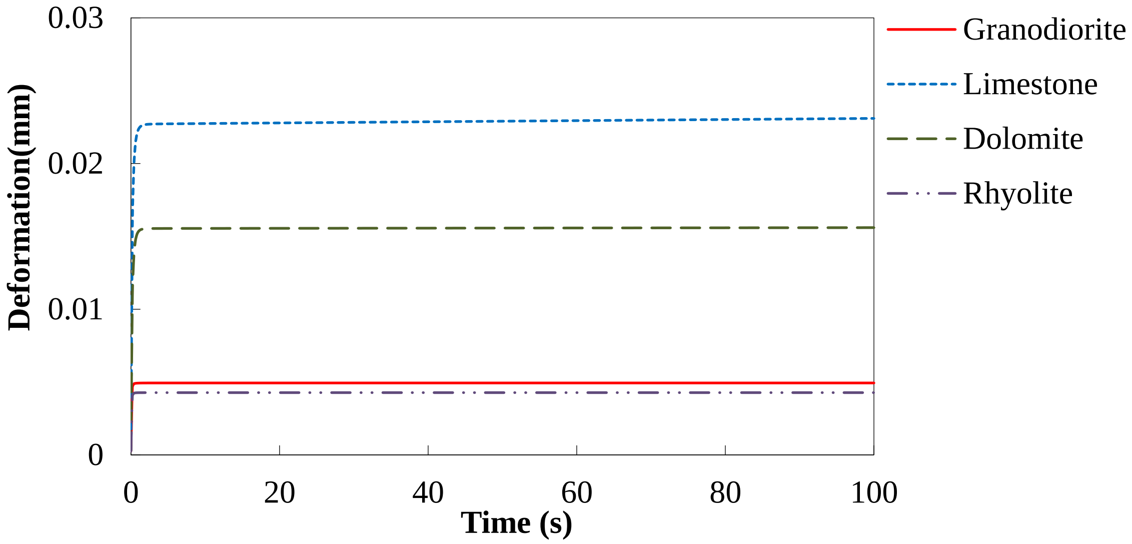

(b)

Figure 3. Image of deformation results: (a) 0°C;(b) 50°C

At 50 °C, the deformations are much smaller than 0 °C because the load amplitude is lower. All the four PA pavements reach at their ultimate deformation values at very early stage, which can ascribe to the lower stiffness of PA mixture at high temperature. The Limestone enhanced PA pavement has the highest deformation value amongst the four filler types, followed by Dolomite and Granodiorite pavement, and Rhyolite pavement has the smallest deformation value. The deformation of Limestone and Dolomite enhanced pavements are 0.0231 mm and 0.0156 mm, respectively, more than three times of that with Granodiorite (0.00494 mm) and Rhyolite fillers (0.00427 mm). The results demonstrate that the load-bearing capacities of pavements with Granodiorite and Rhyolite fillers are close and much higher than the other two fillers at high temperature. The Limestone filler enhanced pavement shows the smallest capacity.

3.2. Rutting resistance of PA pavement at high temperature

The rutting resistance property of asphalt pavement can be predicted by the creep strain distribution. The rutting distress would occur in pavements when the creep strain is relatively higher. The location of the maximum creep strain is identical for the four types of pavements with different fillers, and **Figure 4** exhibits the location of the maximum creep strain in pavement with Granodiorite filler at 50 °C.

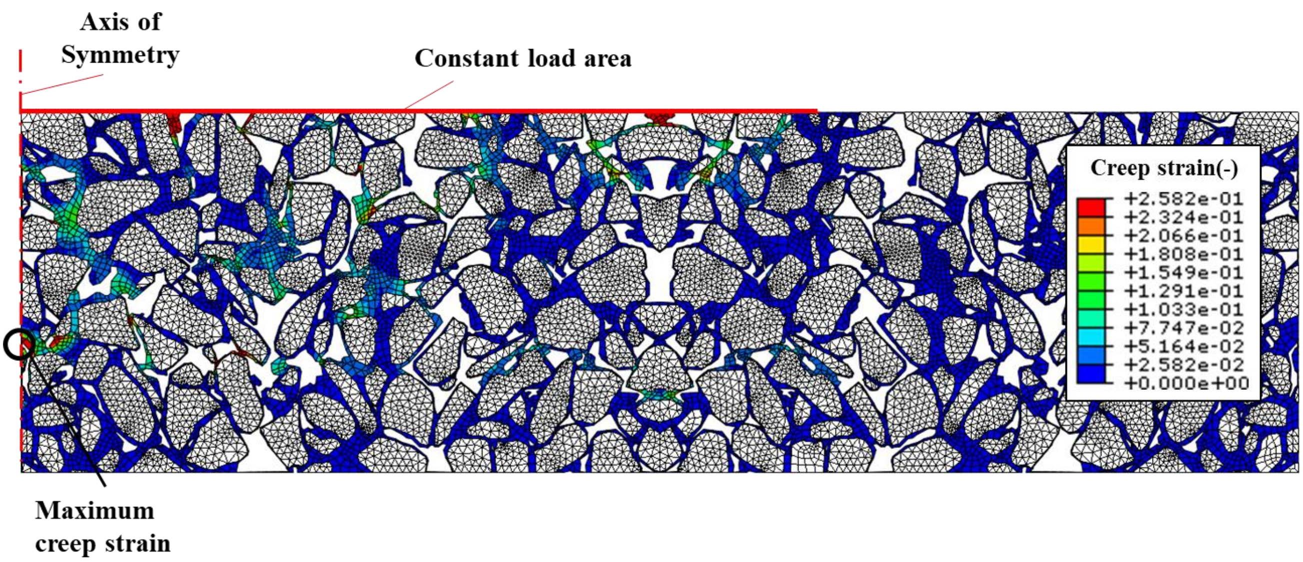

Figure 4. Image of the maximum creep strain location in pavement with Granodiorite filler at 50 °C

The maximum creep strain locates in the axis of the symmetry, which is closely related to the rutting distress of pavements. The significant creep strains mostly distribute under the loading area, especially near the surface of the pavement. Remarkable concentrations appear at the clearance between two aggregates, in which distresses can occur. The maximum creep strain values of the pavements with different fillers at 50 °C were calculated and illustrated in **Figure 5**.

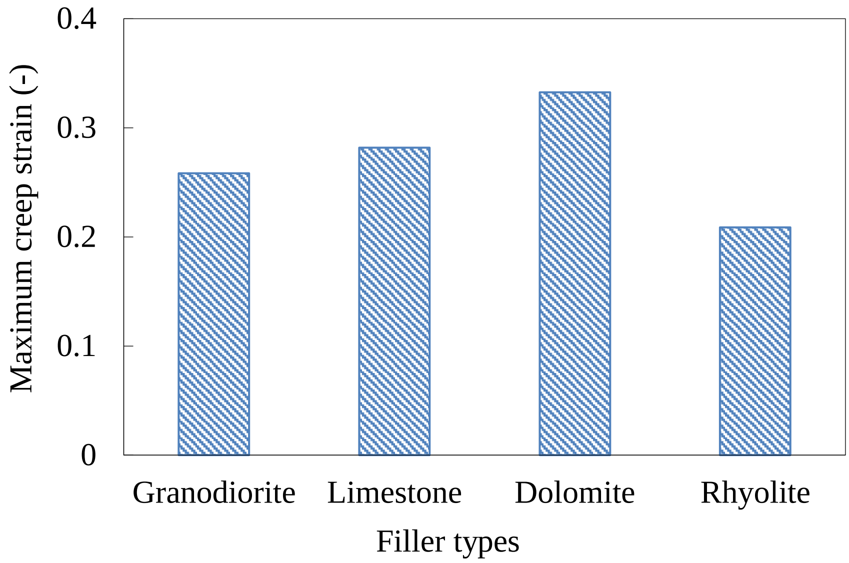

Figure 5. Image of the maximum creep strain at 50 °C

The maximum creep strain of pavement with Dolomite filler has a relatively higher value than that with the other three fillers, indicating the rutting distress would most probably initiate in this pavement. The smallest strain value appears in the Rhyolite enhanced PA pavement, which can be ascribe to the high capacity of this pavement.

3.3 Raveling resistance of pavement at low temperature

The von Mises stress is used to demonstrate the raveling resistance of PA pavement at low temperature (Zhang et al. 2017). The higher von Mises stress values are caused by higher stress concentration in which raveling distress can easily occur. Similarly, the von Mises stress distributions were identical for the pavements with the four mineral fillers. Hence, the von Mises stress distribution in mastic of the pavement with Granodiorite filler at 0 °C is illustrated in **Figure 6**.

Within this figure, the remarkable von Mises stresses mostly distribute under the loading area, and stress concentrations appear between two aggregates. Four specific positions with remarkable von Mises stress concentration are selected as the critical positions for raveling distress. Particularly, the stress in position 2 is more significant than the other positions. The above results demonstrate that the raveling distress can occur in the small clearance of aggregate under the loading area in PA pavements, and the position 2 is more vulnerable than the other positions in subjecting the cracking distress.

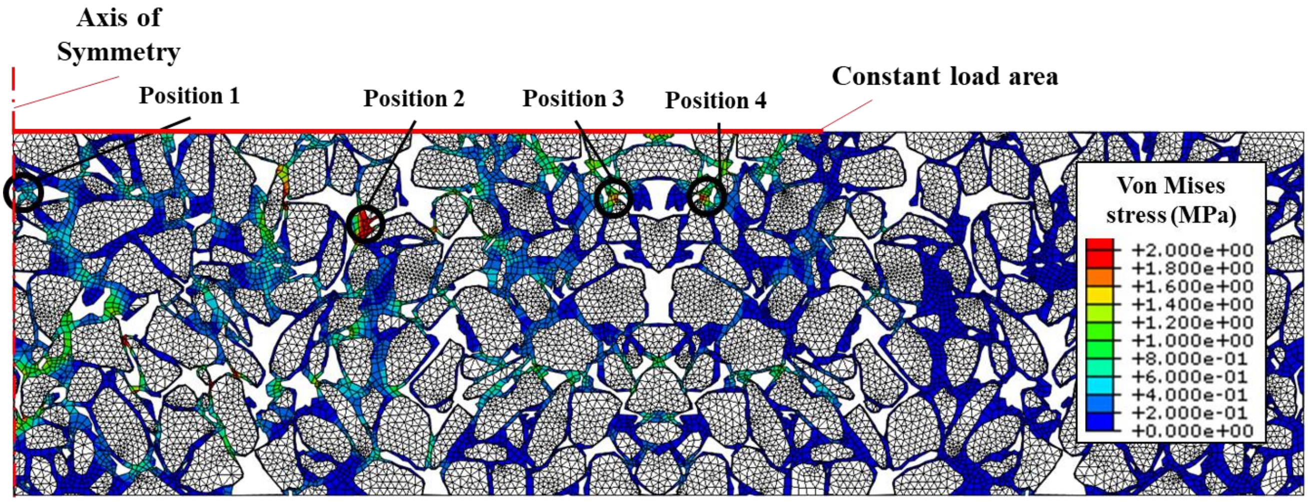

Figure 6. Image of critical locations of von Mises stress in pavement with Granodiorite filler at 0 °C

In addition, the mechanical responses of the pavements with different fillers exhibit significant time-dependent characterization, and therefore, the von Mises stress values for these four positions of PA pavements at various loading times are calculated and presented in **Figure 7**.

At the beginning of the loading (time=1s), the von Mises stress values of different fillers enhanced pavements derived from the same location are close to each other, furthermore, the maximum value of stress locates in position 2 is much higher than the other three positions. The stress values in position 3 and position 4 are close, and the position 1 has the smallest stress value in each pavement. Amongst the four different fillers, the highest and lowest stress values appear in pavements with Granodiorite and Rhyolite fillers, respectively, as shown in **Figure 7 (a)**.

As the loading time increase, the values of von Mises stress decrease especially for the pavements with Limestone and Dolomite fillers. At the end of the loading period (time=100s), the Rhyolite enhanced pavement has the largest von Mises stress, followed by Granodiorite, Limestone and Dolomite fillers enhanced pavements. Moreover, the difference of stress at the four positions in pavement with Dolomite filler is smaller than that with other three fillers, as shown in **Figure 7 (b)**.

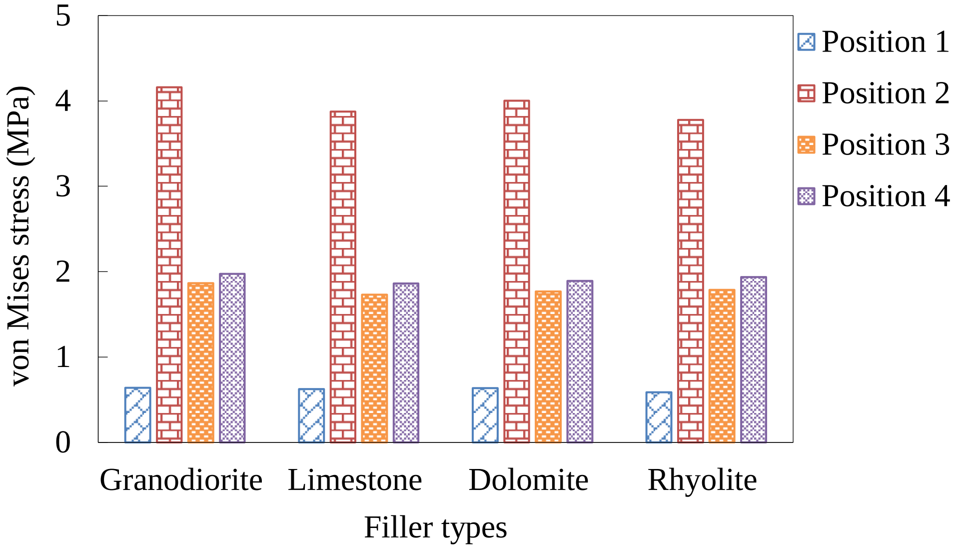

(a)

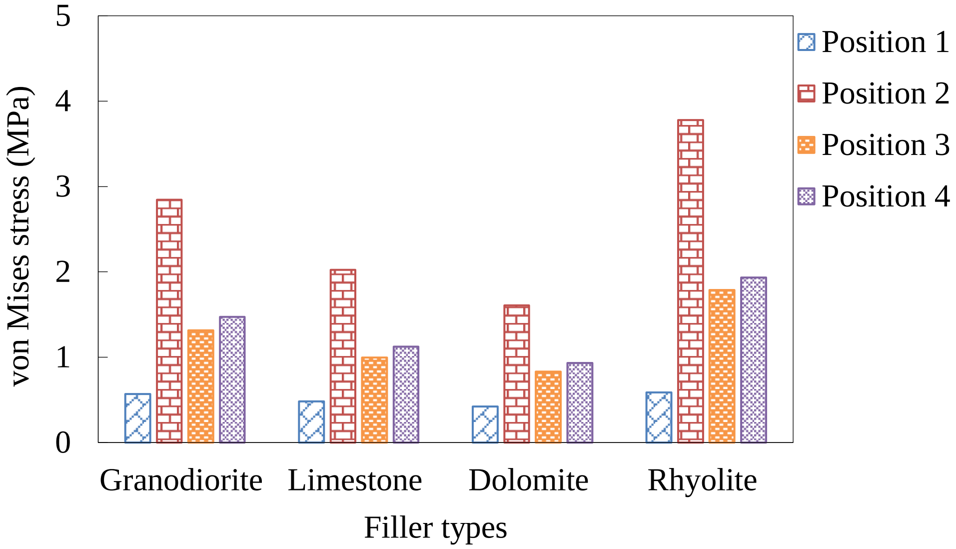

(b)

Figure 7. Values of von Mises stress in the pavement at 0°C: (a) Time=1s; (b) Time=100s.

At low temperature, even though the mechanical behavior of PA mixture is close to the linear elastic, the responses to the cumulative tire loading exhibit remarkable time-dependent characteristic. The raveling resistances of pavements with fillers are different at different loading time. At the early stage of the loading period, the Rhyolite filler enhanced pavement has a relatively higher raveling resistance than others while that of Granodiorite filler enhanced pavement is lower. However, as the increase of the loading time, the von Mises stress values of the pavements decrease due to the stress relaxation of the PA mixture. At the later stage of the loading period, the pavement with Dolomite and Rhyolite respectively witnesses the highest and lowest raveling resistance. In addition, the small stress variation between the four positions in the pavement with Dolomite filler at the end of the loading time indicates that the Dolomite enhanced pavement becomes more flexible as the increase of the loading time, and thus has higher raveling resistance at the later stage of loading.

3.4. Performance ranking and correlation analysis

From the above simulation results, the performances of PA pavements respectively with the four mineral fillers at low and high temperatures are identified. To make a comprehensive evaluation of the four filler types based on the PA pavement performance, the radar graph was employed in this study, as shown in **Figure 8**. The radar graph is structured that an improvement in a material property can be expected with an increasing distance from the axis cross. Hence, the PA pavements with different fillers cover different areas in the diagram. In this study, four performances of PA pavement, i.e., load-bearing capacity at low temperature, load-bearing capacity at high temperature, rutting resistance at high temperature and raveling resistance at low temperature, were evaluated. Noted that each of the three indexes (deformation, creep strain and von Mises stress) has a negative correlation with the performances of pavements (load-bearing capacity, rutting resistance and raveling resistance), and therefore, for each performance, the reciprocal of the index was calculated and analyzed herein.

It is illustrated that the pavements with Rhyolite and Granodiorite fillers show the higher load-bearing capacity and rutting resistance, whilst the pavements with Dolomite and Limestone fillers have better raveling resistance. In conclusion, the PA mixture with Rhyolite and Granodiorite fillers are suitable for pavements under high temperature and standing heavy traffic; and the PA pavements with Limestone and Dolomite fillers have better anti-raveling performance.

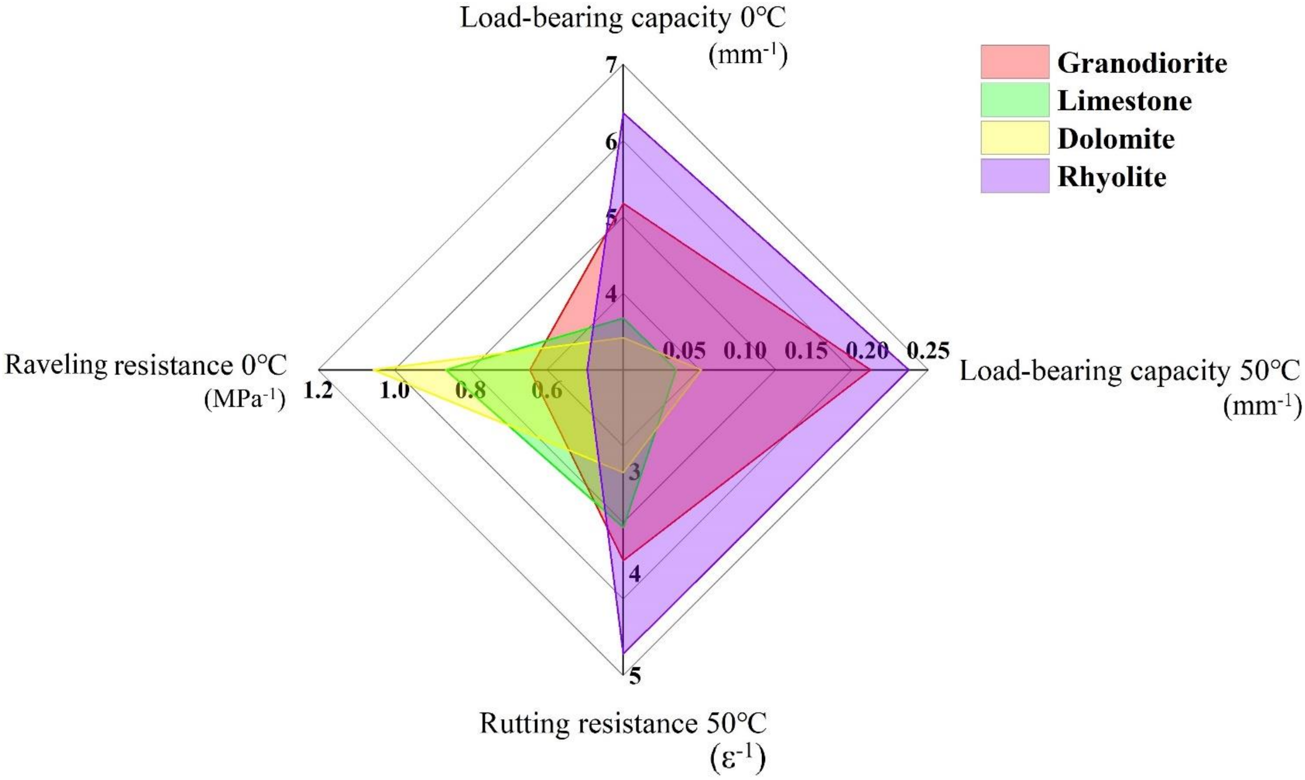

Figure 8. Diagram for the PA pavements with different fillers

In order to quantify the relationship between the chemical content of mineral filler and performance of PA pavement, the Pearson correlation coefficients were calculated and listed in **Table 5**, which represents the linear relation between the two variables. The range of the coefficients is between -1.0 and 1.0, which respectively denotes the negative and positive correlation. When the coefficient values approach to 0.0, the correlations between two variables get weaker; the coefficient values of 0.0 denote that there are no correlations between two variables.

Table 5. Pearson correlation coefficients

	Na_2O	MgO	Al_2O_3	SiO_2	K_2O	CaO	TiO_2	Fe_2O_3
Load-bearing capacity 0°C	0.614	-0.640	0.950	0.945	0.965	-0.884	0.418	0.538
Load-bearing capacity 50°C	0.776	-0.525	0.996	0.995	0.895	-0.976	0.602	0.735
Rutting resistance 50°C	0.427	-0.754	0.831	0.824	0.941	-0.710	0.237	0.316
Raveling resistance 0°C	-0.645	0.813	-0.917	-0.914	-0.884	0.798	-0.487	-0.537

It can be seen from **Table 5** that the components of Al_2O_3, SiO_2, K_2O and CaO show the most significant relationships with the PA pavement performance. In addition, the chemical components of Na_2O, MgO and Fe_2O_3 also exhibit strong relationships with some of the PA pavement performances.

To clearly illustrate and compare the correlations, the Pearson correlation coefficients are presented in **Figure 9**. Within this figure, the components with coefficient values higher than 0.8 are regarded to have significant correlations, and the chain-dotted lines denote the coefficient values equal to 0.8 and -0.8.

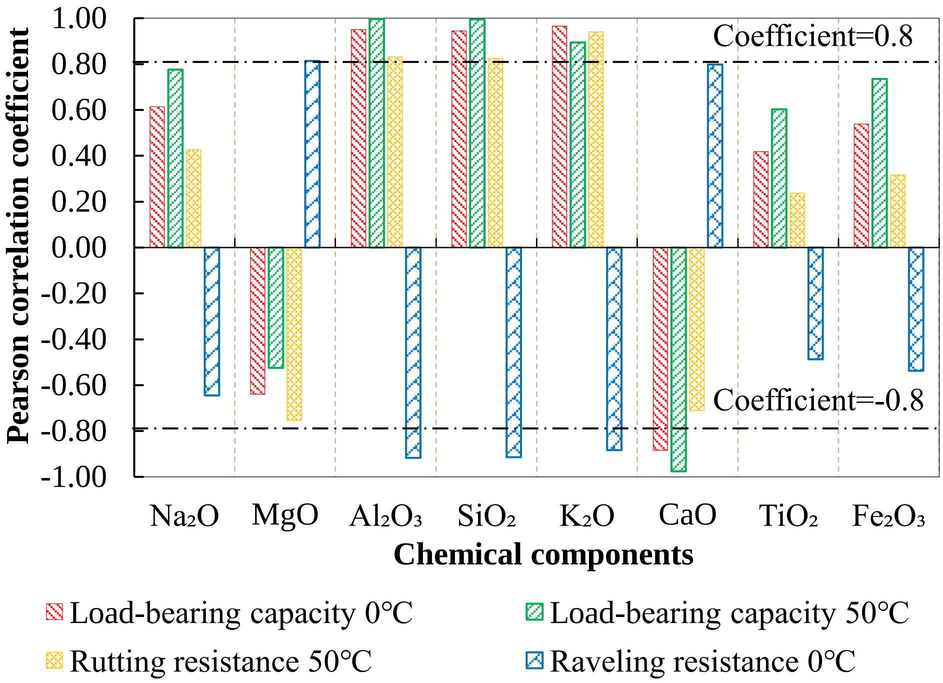

Figure 9. Image of Pearson correlation coefficients

It can be observed that the chemical components of Na_2O, Al_2O_3, SiO_2, K_2O, TiO_2 and Fe_2O_3 exhibit the positive correlations with the load-bearing capacity and rutting resistance, and the negative correlations with the raveling resistance of PA pavement. However, the mass components of Na_2O, K_2O, TiO_2 and Fe_2O_3 are relatively small (much less than Al_2O_3 and SiO_2), and thus only the chemical components of Al_2O_3 and SiO_2 are considered to play dominate roles in improving the load-bearing capacity and rutting resistance of PA mixture as well as PA pavements.

On the other hand, the chemical components of MgO and CaO show the positive correlations with the raveling resistance and the negative correlations with load-bearing capacity and rutting resistance. The mass component as well as the correlation of CaO is much higher than that of MgO. Hence, it can be concluded that the fillers with high percentages of CaO can reduce the load-bearing capacity and rutting resistance of PA pavements; while the raveling resistance of PA pavements can be improved by more CaO component.

4. Conclusions and outlook

The present study develops a coupled multiscale model to investigate the effects of mineral fillers on the performance of PA pavements. Within this model, the mesoscale model of PA mixture was established from the CT image of the PA specimen based on the DIP technology. Four types of asphalt mastic were prepared respectively with different mineral fillers (Granodiorite, Limestone, Dolomite and Rhyolite), and their linear viscoelastic properties at 0 °C and 50 °C were specified in the simulation. A constant loading was applied on the model to simulate the cumulative tire loadings. As a result, the performances of PA pavements with different fillers were obtained and ranked, and the correlations between pavement performance and chemical components of fillers were identified.

(1) The heterogeneous structure of PA mixture causes significant stress or strain concentrations in mixture especially between two aggregate particles, which makes it difficult to precisely predict the mechanical response of PA pavements.

(2) The pavements with Rhyolite and Granodiorite fillers have relatively higher load-bearing capacities under lower and higher temperatures.

(3) At high temperature, the Rhyolite filler can more effectively improve the rutting resistance of PA pavement, while the pavement with Dolomite filler would be the vulnerable when subjecting to the rutting distress.

(4) Although the properties of PA mixture are close to linear elasticity at low temperature, remarkable time-dependent responses can still be observed in the deformation and von Mises stress distribution of pavements under accumulative loading. At the end of loading period, the pavement with Dolomite filler exhibits the best raveling resistance.

(5) The correlation analyses demonstrate that the components of Al_2O_3 and SiO_2 can effectively improve the load-bearing capacities and rutting resistance of PA pavements, while the

component of CaO can enhance the raveling resistance of PA pavements.

The different mineral fillers significantly influence the mechanical response of the PA pavements. The abovementioned conclusions contribute to the current knowledge, and based on this algorithm, it is possible to select optimal filler for a specific pavement design. The further investigation needs to be carried out, for example, an intermedium temperature will be adopted in the FE simulation and the fatigue performance of the PA pavements will be simulated and evaluated.

Acknowledgments

The work underlying this project was carried out under the research grant numbers FOR 2089/2 (OE514/1-2, WE 1642/1-2 and LE 3649/1-2) and OE514/4-2, on behalf of the grant sponsor, the German Research Foundation (DFG). as well as the grant number 57446137 funded by German Academic Exchange Service (DAAD) and Universities Australia.

References

Al-Hdabi, A., Al Nageim, H. & Seton, L., 2014. Performance of gap graded cold asphalt containing cement treated filler. *Construction and Building Materials,* 69, 362-369.

Alber, S., Ressel, W., Liu, P., Hu, J., Wang, D., Oeser, M., Uribe, D. & Steeb, H., 2018. Investigation of microstructure characteristics of porous asphalt with relevance to acoustic pavement performance. *International Journal of Transportation Science and Technology,* 7 (3), 199-207.

Allen, D.H., 2001. Homogenization principles and their application to continuum damage mechanics. *Composites Science and Technology,* 61 (15), 2223-2230.

Alvarez, A.E., Gomez, K.L., Gomez, D.C. & Reyes-Ortiz, O.J., 2019. Optimising the effect of natural filler on asphalt-aggregate interfaces based on surface free energy measurements. *Road Materials and Pavement Design,* 20 (7), 1548-1570.

Alvarez, A.E., Martin, A.E. & Estakhri, C., 2011. A review of mix design and evaluation research for permeable friction course mixtures. *Construction and Building Materials,* 25 (3), 1159-1166.

Cardone, F., Frigio, F., Ferrotti, G. & Canestrari, F., 2015. Influence of mineral fillers on the rheological response of polymer-modified bitumens and mastics. *Journal of Traffic and Transportation Engineering (English Edition),* 2 (6), 373-381.

Dai, Q., Sadd, M.H., Parameswaran, V. & Shukla4, A., 2005. Prediction of damage behaviors in asphalt materials using a micromechanical finite-element model and image analysis. *Journal of Engineering Mechanics,* 131, 668-677.

Fgsv, 2007. Asphalt-stb, z. T. V. . *Zusätzliche Technische Vertragsbedingungen und Richtlinien für den Bau von Verkehrsflächenbefestigungen aus Asphalt.* Köln.

Fonseca, J.F., Teixeira, J., Branco, V. & Kim, Y.R., 2019. Evaluation of effects of filler by-products on fine aggregate matrix viscoelasticity and fatigue-fracture characteristics. *Journal of Materials* *in Civil Engineering,* 31 (10), 10.

Forschungsgesellschaft Für Straßen- Und Verkehrswesen, A.A., 1999. Technische prüfvorschriften für asphalt im straßenbau *TP A-StB.*

Kim, Y.-R., Souza, F.V. & Teixeira, J.E.S.L., 2012. A two-way coupled multiscale model for predicting damage-associated performance of asphaltic roadways. *Computational Mechanics,* 51 (2), 187-201.

Kim, Y.R. & Little, D.N., 2004. Linear viscoelastic analysis of asphalt mastics. *Journal of Materials in Civil Engineering,* 16 (2), 122-132.

Kollmann, J., Lu, G., Liu, P., Xing, Q., Wang, D., Oeser, M. & Leischner, S., 2019. Parameter optimisation of a 2d finite element model to investigate the microstructural fracture behaviour of asphalt mixtures. *Theoretical and Applied Fracture Mechanics,* 103.

Li, X., Lv, X., Liu, X. & Ye, J., 2019. Discrete element analysis of indirect tensile fatigue test of asphalt mixture. *Applied Sciences,* 9 (2), 327.

Liu, P., Hu, J., Wang, H., Falla, G., Wang, D. & Oeser, M., 2018a. Influence of temperature on the mechanical response of asphalt mixtures using microstructural analysis and finite-element simulations. *Journal of Materials in Civil Engineering,* 30.

Liu, P., Xu, H., Wang, D., Wang, C., Schulze, C. & Oeser, M., 2018b. Comparison of mechanical responses of asphalt mixtures manufactured by different compaction methods. *Construction and Building Materials,* 162, 765-780.

Liu, Q.T., Garcia, A., Schlangen, E. & Van De Ven, M., 2011. Induction healing of asphalt mastic and porous asphalt concrete. *Construction and Building Materials,* 25 (9), 3746-3752.

Liu, Q.T., Schlangen, E., Van De Ven, M., Van Bochove, G. & Van Montfort, J., 2012. Evaluation of the induction healing effect of porous asphalt concrete through four point bending fatigue test. *Construction and Building Materials,* 29, 403-409.

Lu, G.Y., Liu, P.F., Wang, Y.H., Fassbender, S., Wang, D.W. & Oeser, M., 2019a. Development of a sustainable pervious pavement material using recycled ceramic aggregate and bio-based polyurethane binder. *Journal of Cleaner Production,* 220, 1052-1060.

Lu, G.Y., Renken, L., Li, T.S., Wang, D.W., Li, H. & Oeser, M., 2019b. Experimental study on the polyurethane-bound pervious mixtures in the application of permeable pavements. *Construction and Building Materials,* 202, 838-850.

Mohd Shukry, N.A., Abdul Hassan, N., Abdullah, M.E., Hainin, M.R., Yusoff, N.I.M., Mahmud, M.Z.H., Putra Jaya, R., Warid, M.N.M. & Mohd Satar, Mohd k.I., 2018. Influence of diatomite filler on rheological properties of porous asphalt mastic. *International Journal of Pavement Engineering,* 21 (4), 428-436.

Qian, N., Wang, D., Li, D. & Shi, L., 2020. Three-dimensional mesoscopic permeability of porous asphalt mixture. *Construction and Building Materials,* 236.

Reyes-Ortiz, O.J., Mejia, M. & Useche-Castelblanco, J.S., 2019. Aggregate segmentation of asphaltic mixes using digital image processing. *Bulletin of the Polish Academy of Sciences-Technical Sciences,* 67 (2), 279-287.

Rieksts, K., Pettinari, M. & Haritonovs, V., 2018. The influence of filler type and gradation on the rheological performance of mastics. *Road Materials and Pavement Design,* 20 (4), 964-978.

Roberto, A., Romeo, E., Montepara, A. & Roncella, R., 2020. Effect of fillers and their fractional voids on fundamental fracture properties of asphalt mixtures and mastics. *Road Materials and Pavement Design,* 21 (1), 25-41.

Rochlani, M., Leischner, S., Falla, G.C., Wang, D., Caro, S. & Wellner, F., 2019. Influence of filler properties on the rheological, cryogenic, fatigue and rutting performance of mastics. *Construction and Building Materials,* 227.

Stewart, C.M. & Garcia, E., 2019. Fatigue crack growth of a hot mix asphalt using digital image correlation. *International Journal of Fatigue,* 120, 254-266.

Sun, Y., Du, C., Gong, H., Li, Y. & Chen, J., 2020. Effect of temperature field on damage initiation in asphalt pavement: A microstructure-based multiscale finite element method. *Mechanics of Materials,* 144, 103367.

Sun, Y., Du, C., Zhou, C., Zhu, X. & Chen, J., 2019. Analysis of load-induced top-down cracking initiation in asphalt pavements using a two-dimensional microstructure-based multiscale finite element method. *Engineering Fracture Mechanics,* 216, 106497.

Wang, H., Wang, J. & Chen, J., 2014. Micromechanical analysis of asphalt mixture fracture with adhesive and cohesive failure. *Engineering Fracture Mechanics,* 132, 104-119.

Wollny, I., Hartung, F., Kaliske, M., Liu, P., Oeser, M., Wang, D., Canon Falla, G., Leischner, S. & Wellner, F., 2020. Coupling of microstructural and macrostructural computational approaches for asphalt pavements under rolling tire load. *Computer-Aided Civil and Infrastructure Engineering*.

Xing, C., Xu, H.N., Tan, Y.Q., Liu, X.Y., Zhou, C.H. & Scarpas, T., 2019. Gradation measurement of asphalt mixture by x-ray ct images and digital image processing methods. *Measurement,* 132, 377-386.

Yin, A., Yang, X., Gao, H. & Zhu, H., 2012. Tensile fracture simulation of random heterogeneous asphalt mixture with cohesive crack model. *Engineering Fracture Mechanics,* 92, 40-55.

Zhang, D., Gu, L. & Zhu, J., 2019. Effects of aggregate mesostructure on permanent deformation of asphalt mixture using three-dimensional discrete element modeling. *Materials (Basel),* 12 (21).

Zhang, Y. & Leng, Z., 2017. Quantification of bituminous mortar ageing and its application in ravelling evaluation of porous asphalt wearing courses. *Materials & Design,* 119, 1-11.